Mn Doped ZnO Film for Ethanol Vapor Detection

N. Neupane, R. Ghimire, D. R. Gibbs, S. P. Shrestha, S. Dhakal, D. D. Mulmi and L. Pradhan Joshi

Journal of Nepal Physical Society

Volume 9, Issue 2, December 2023

ISSN: 2392-473X (Print), 2738-9537 (Online)

JNPS, **9** (2): 7-13 (2023)

DOI: https://doi.org/10.3126/jnphyssoc.v9i2.62284

Published by:

Nepal Physical Society
P.O. Box: 2934
Tri-Chandra Campus
Kathmandu, Nepal
Email: nps.editor@gmail.com

JNPS 9 (2): 7-13 (2023)
ISSN: 2392-473X (Print), 2738-9537 (Online)

Research Article *© Nepal Physical Society*
DOI: https://doi.org/10.3126/jnphyssoc.v9i2.62284

Mn Doped ZnO Film for Ethanol Vapor Detection

N. Neupane[1], R. Ghimire[2], D. R. Gibbs[3], S. P. Shrestha[2], S. Dhakal[3], D. D. Mulmi[4]* and L. Pradhan Joshi[1,]*

[1]Department of Physics, Amrit Campus, Tribhuvan University, Kathmandu, Nepal
[2]Department of Physics, Patan Multiple Campus, Tribhuvan University, Kathmandu, Nepal
[3]Virginia Commonwealth University, Department of Chemistry, Richmond, VA, 23284, USA
[4]Nanomaterials Research Laboratory, Nepal Academy of Science & Technology, Khumaltar, Nepal
*Corresponding Email: deependra.mulmi@nast.gov.np, leela.pradhanjoshi@ac.tu.edu.np

Received: *12th June, 2023;* ***Revised:*** *29th October, 2023;* ***Accepted:*** *20th November, 2023*

ABSTRACT

It has become a major challenge to develop highly sensitive and selective ZnO gas sensors to detect the leakage of toxic and explosive gases due to their high operating temperature. This article reports the design, characterization, and application of a Mn-doped ZnO thin film for ethanol gas vapor detection at a relatively lower temperature. To achieve this, undoped (0%) and Mn doped ZnO thin films were prepared using a spin coating technique and their structural, morphological and optical characterizations were carried out using XRD, SEM, EDX and UV-vis spectrophotometer. The XRD analysis showed a polycrystalline ZnO structure with the preferred orientations along (100), (002), (101), (102), (110), (103), and (200) planes. Upon Mn doping, the average crystallite size and band gap of ZnO were found to be decreased, which indicated that Mn ions substitute into the lattice of ZnO. Interestingly, SEM images revealed the grainy like porous ZnO surfaces. The EDX results confirmed the presence of Mn dopant in the ZnO lattice. In the doped films, the changes in particle size and grain boundaries of nanocrystalline ZnO resulted changes in sensitivity and operating temperature of ZnO gas sensor. The sensitivity measurements towards ethanol vapor showed significant decrease of the operating temperature from 220^{o}C to 160^{o}C as Mn concentration was increased from 0 to 5%. As-prepared Mn-doped ZnO sensors will be useful for sensing ethanol vapor at relatively low temperature.

Keywords: Band gap, Ethanol vapor detection, Operating temperature, Sensitivity, ZnO sensor.

1. INTRODUCTION

The rapid development of industrial civilization requires monitoring of harmful gases in order to protect human health and the environment. For this purpose, metal oxide semiconductors such as ZnO have gained much research interest [1]. Much effort has been devoted to develop highly sensitive, selective, fast responsive, and fully recyclable gas sensors for the detection of toxic and explosive gases including ethanol [2, 3]. It has been realized that, sensor that can allow precise identification of ethanol vapor, can have a tremendous applications both in research labs and industries.

In recent years, ZnO has emerged as a potential metal oxide compound in a myriad of applications: a transparent conducting material for solar cells, ultra-violet laser and nanotechnology device fabrications, optoelectronics for smart windows, piezoelectric device preparation and gas sensors [4-7]. ZnO thin films have attracted considerable attention for these applications because of its moderately high electron mobility, high infrared reflectance and visible transmittance, large exciton binding energy (60 meV), radiation hardness, and biocompatibility [3-7]. Additionally, ZnO films are being utilized in gas sensing because of their tunable surface morphologies upon doping [8]. Along this line, recent studies have shown that the performance of ZnO gas sensors can be improved by metal and transition metal doping [9-11]. Another critical parameter to consider is the

development of grain boundaries during preparation of ZnO films, which plays an important role in carrier transport properties within grain and grain boundaries of the films [12]. This is because the traps within or at grain boundaries of nanocrystalline ZnO capture free electrons from the adjoining grains resulting in the electrons accumulation at the grain boundary region, which creates charged defect states and acts as a carrier scattering centre. As a result, the conductivity of the films decreased [13].

In recent nanotechnology, use of metal oxide nanostructures in sensing devices is a promising new direction. Based on the literature, undoped and transition metal doped ZnO films can be prepared using various physical and chemical deposition techniques such as magnetron sputtering [14], chemical vapor deposition [15], laser ablation [16], sol-gel [17], spray pyrolysis [18], hydrothermal growth [19] and spin coating [20]. But most of these methods utilize low pressure, high temperature, controlled rate of flow of carrier gas etc. In this work we have synthesized undoped and Mn doped grainy like surfaced ZnO thin films using a spin coating method as it allows the production of a film which is highly stable and tightly adhered to its substrate at low cost and highly reproducible manner. Using thus-prepared thin films, the effect of Mn doping concentration on sensitivity of measurements of ethanol vapor in the temperature range from room temperature to 300^{o}C was investigated [21]. In addition, they are both rapidly responsive and highly recyclable making it a good candidate for the development of next generation gas sensors.

2. EXPERIMENTAL

2.1 Materials

All the chemicals used in the experiment were of analytical grade and consumed without further purification. They include Zinc Acetate Dihydrate, Zn $(CH_3COO)_2.2H_2O$, ≥98.5%, (Qualigens fine chemicals); Diethanolamine (DEA), $HN(CH_2CH_2OH)_2$, ≥99% (Thermo Fischer Scientific); Absolute ethanol, ≥ 99.5% (Merck KGaA) and Manganous Chloride Tetrahydrate, Mn $Cl_2.4H_2O$, ≥98.5% (Fischer Scientific). For cleaning glassware and utensils, deionized water was used.

2.2 Deposition of ZnO films

Undoped and Mn doped ZnO thin films were deposited on the glass substrate by the spin coating method. A 0.5M precursor solution was prepared by dissolving Zinc Acetate Dihydrate salt into ethanol along with DEA in a magnetic stirrer, at 60^{o}C for 1 h. The molar ratio of Zinc Acetate and DEA was maintained at 1:1. The solution was filtered using Whatmann filter paper. In another set, the 0.5M dopant solution was prepared by mixing Manganous Chloride Tetrahydrate in to absolute ethanol with continuous stirring at 60^{o}C for 1 h. Doping concentrations was varied from 1 to 5 at. % by adjusting the volumes of Zinc Acetate and Manganous Chloride. This precursor was aged for 24 h to check whether it formed precipitation prior to deposition. The precursor solution was mixed with the dopant solutions before coating on the required proportions. Using the spin coater with rpm set at 3000 for 30 s, thin films of ZnO were deposited. The coated substrates were then soft baked at 200^{o}C for 10 min for each layer followed by hard baking at a high temperature of 550^{o}C for 30 min. Ultimately, after completing the coating, samples were annealed at 2 h in the muffle furnace at 550^{o}C.

2.3 Characterization

The structural characterization of the prepared ZnO films was done using AnalyticalX'Pert Pro X-ray diffractometer of CuKα radiation (wavelength: 1.54 Å). The surface morphology and elemental analysis of the ZnO samples were analyzed using Scanning Electron Microscopy (SEM) (Ultra High-Resolution Analytical FE-SEM SU-70, with platinum sputter coated samples) and Energy Dispersive X-ray (EDX) techniques. The optical transmittance of ZnO samples was captured using UV-Vis spectrophotometer (Carry 60 spectrophotometer, Agilent Technology) from 200 nm to 800 nm to calculate the band gap values.

2.4 Sensing measurement

The sensing experiment was carried out by a homemade set up as shown in the schematic diagram. To characterize the gas-sensing properties of thin films, electrodes were made using silver paste.

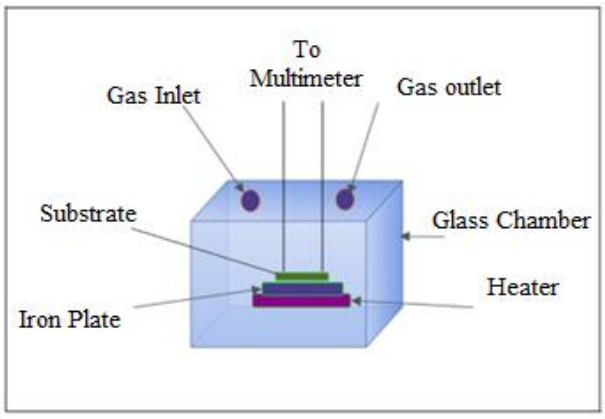

Fig. 1: Schematic diagram of homemade gas sensing setup.

A simple and low-cost gas sensor was designed and fabricated to measure the gas sensing response of ZnO thin films. For temperature dependence of gas response, the set up was equipped with a micro heater using Ni-Cr coil. The gas sensor was kept above the heater. A thermocouple was also fitted in order to monitor the substrate temperature. Ethanol was injected inside the closed glass chamber and made air tight by using the cork. After each injection of the gas, the gas was completely leaked out of the chamber. Response time and recovery time were also measured. The resistance of the film was measured by a multimeter of high mega ohm range. This device was very sensitive even for a small amount of gas and the measurements were reproducible. The sensitivity of the gas sensor was evaluated using the following relation [1]

$$Sensitivity = \frac{(R_a - R_g)}{R_a} \times 100\%$$

where, R_a is the resistance of the sensor in the air and R_g is the resistance in the presence of the gas.

3. RESULTS AND DISCUSSIONS

3.1 Surface morphology and crystal structure

Fig.2 shows the X-ray diffraction pattern of undoped and Mn doped ZnO films with different concentrations as labeled. The XRD pattern consisted of a number of peaks indicating ZnO films were polycrystalline in nature. Interestingly, the peak intensity was decreased and the peak width was increased with increasing the doping concentration. Three intense peaks were observed at 31.24° (100), 33.85° (002) and 35.66° (101) for undoped ZnO film that were found to be consistent with the ZnO peaks of JCPDS card number 36-1451 [22]. Additionally, less intense peaks of (102), (110), (103), and (200) were also present. Similar sets of peaks were observed for Mn doped ZnO samples as shown in fig. 2.

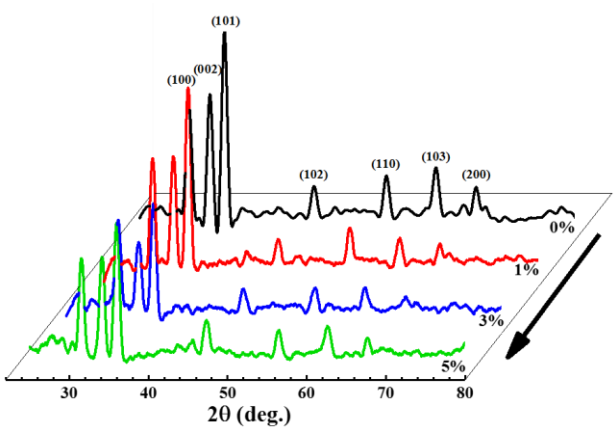

Fig. 2: (color online) XRD pattern of undoped and Mn doped ZnO.

In 3% Mn-doped sample, the intensity of (002) peak is significantly decreased. The crystallite size (D) of ZnO was estimated using the Debye Scherer's formula. The average crystallite size of Mn-dopped ZnO was found smaller than for the undoped sample. These results suggest that there is incorporation of Mn in the ZnO and reduction in the crystallinity of the films [23-24]. The calculated interplanar spacing (d) along with the crystallite size is shown in Table 1.

Table 1: Comparison of calculated d spacing with standard JCPDS d-spacing and grain sizes.

Mn-Doping in at. %	Angle 2θ (degree)	Calculated d (Å)	JCPDS d (Å)	Crystallite Size D (Å)	Average D (nm)
0%	31.24	2.8645	2.8142	117.65	
	33.85	2.6494	2.6033	121.92	**11.9±0.3**
	35.66	2.5189	2.4759	116.76	
1 %	31.24	2.8627	2.8142	113.73	
	33.83	2.6469	2.6033	107.82	**10.9±0.4**
	35.74	2.5134	2.4759	107.03	
3%	31.51	2.8405	2.8142	106.25	
	34.18	2.6245	2.6033	99.40	**10.4±0.4**
	36.01	2.4952	2.4759	107.73	
5%	31.54	2.8406	2.8142	119.13	
	34.15	2.6268	2.6033	105.82	**10.9±0.8**
	35.97	2.4979	2.4759	103.52	

3.2 Surface Morphology and Elemental Analysis:

Fig. 3(a), 3(b) and 3(c) show the SEM images of undoped, 1% Mn doped and 3% Mn doped ZnO films respectively. The SEM images depict grainy like structure of ZnO with decrease in particle size for Mn doped into ZnO. Insets in each figure show the SEM images captured at 100 nm resolution.

Fig. 4(a) and 4(b) illustrate the EDX spectra of undoped and 1% Mn doped ZnO thin films. The presence of Mn, Zn and O was confirmed by the occurrence of their respective peaks in Mn-doped ZnO thin films. The other two peaks of Ca and Si originated from the constituents of the glass substrate. The graph clearly demonstrates that Mn was well incorporated into the ZnO film.

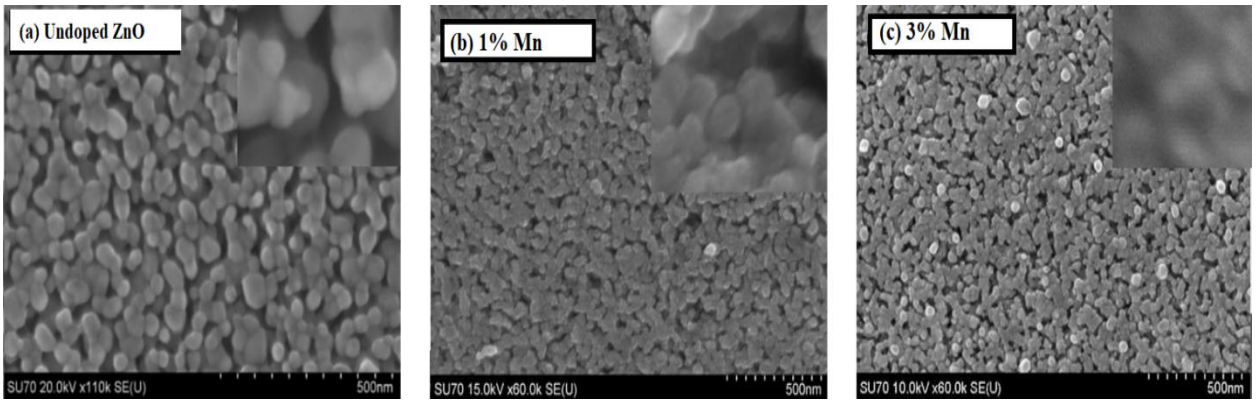

Fig. 3: SEM images of Undoped,1% and 3% Mn doped ZnO.
Insets in each figures show the SEM images captured at 100 nm resolution.

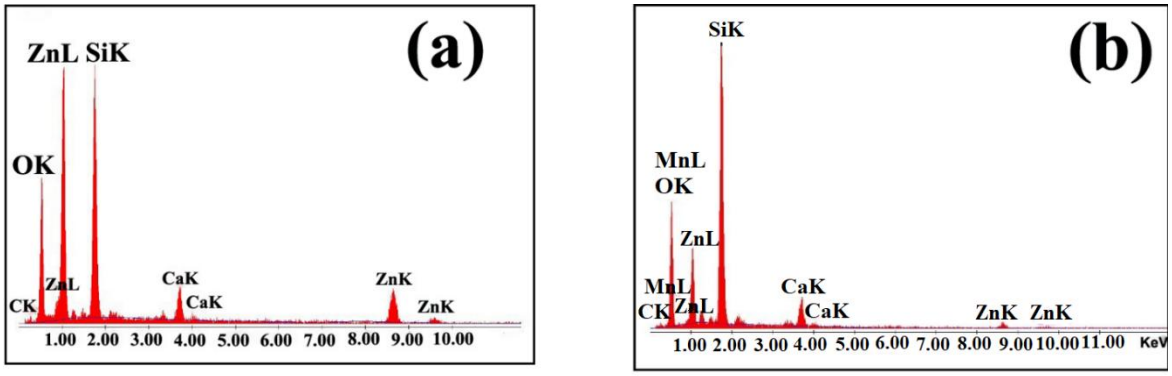

Fig. 4: EDX spectrum of (a) undoped ZnO (b) 1% Mn doped ZnO film.

3.3 Optical Properties

A graph of $(\alpha h\nu)^2$ versus photon energy(hv) was plotted in order to estimate the band gap energy (E_g) shown in Fig 5. By extrapolating the linear portion of each graph, the band gaps of undoped and Mn doped ZnO films were determined. The results illustrated the red shift in band gap value due to Mn doping. The band gap was found to be decreased from 3.28 eV for undoped to 3.13 eV for 5% Mn doping film as shown in the inset of Fig. 5. This narrowing of the band gap by increasing the Mn content is attributed to the exchange interaction between the 'd' electron of Mn atom and 's' and 'p' electrons of the host Zn atom (s-d and p-d interactions) [25].

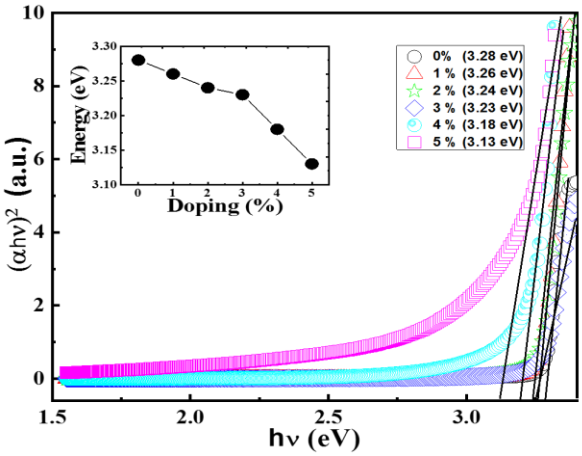

Fig. 5: Band gap of undoped and Mn doped ZnO, inset shows the decreased band gap for Mn doped ZnO.

3.4 Sensor Application

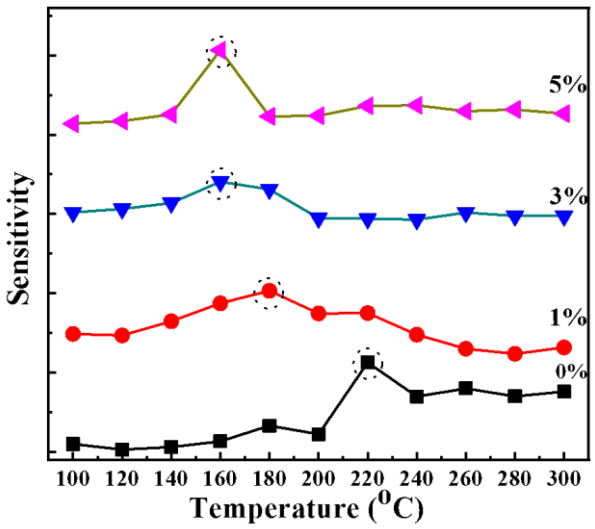

Fig. 6: (color online) Sensitivity of Undoped and Mn doped ZnO films measured at 1000 ppm of ethanol vapor. The dotted circles represent the optimum operating temperature for different Mn concentrations.

Fig. 6 shows the sensitivity measurement of undoped and Mn doped ZnO for ethanol gas vapor using a homemade gas sensing setup in the temperature range from 100°C to 300°C. In this experiment, the concentration of ethanol injected is 1000 ppm. The sensitivity was calculated by measuring the change in resistance of all samples in air (R_a) and gas (R_g) [26]. Here R_g is found to be smaller than R_a for all samples. The resistance of all the ZnO samples was decreased for increasing the temperature. The required activation energy for the adsorption of gas molecules on their surface is supplied by heat. The optimum operating temperatures for different concentrations of Mn are marked by the dotted circles in Fig. 6. The optimum temperature depends on the sensing material and the nature of the gases to detect. The strength of the van der Waals bond between the material and the gas is the most important factor to determine at what temperature to operate the sensor. In the present work, the highest sensitivity of 56% was observed at 220°C for undoped ZnO and the lowest sensitivity of 26% for 3% Mn doped sample at 160°C. The systematic decrease in operating temperature was observed from 220°C for undoped to 160°C for the 3% Mn doped ZnO film. It was saturated at 160°C on further increasing the Mn concentration upto 5%. Upon further augmenting the concentration, the resistance began to increase. This may be due to the defects introduced in the host ZnO.

3.5 Response and Recovery Time

The time response of undoped and Mn doped ZnO films is illustrated in Fig. 7(a) through 7(d). Two cycles of ethanol injection were performed at the operating temperature of 220°C for undoped ZnO as shown in Fig. 7(a). The response time (the time taken to obtain a stable signal) [26] for the first injection of ethanol was observed to be 150 s while the recovery time (time required for 90% of the resistance change) [27] was 299 s. For the second injection of ethanol the response time was about 72 s and the recovery time was 119 s. The response and recovery time were decreased for Mn doped samples. The process was continued with 1, 3, and 5% Mn doped samples with respective operating temperatures and similar trends were found, which are shown in Fig. 7(b), 7(c) and 7(d) respectively.

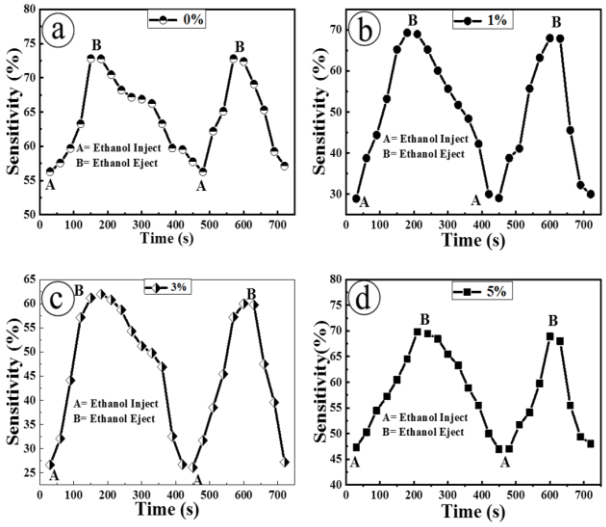

Fig. 7: Response and Recovery Time of (a) 0% (b) 1% (c) 3% (d) 5% Mn doped ZnO.

3.6 Sensing mechanism with model:

The ZnO sensor detects a change in resistance when gas molecules react to its surface. In an ambient environment, oxygen molecules are adsorbed on the surface of ZnO and then ionize into oxygen species by capturing electrons from the conduction band, leading to the formation of a surface depletion layer and thus increasing the sensor resistance [28]. When ethanol approaches the ZnO surface, the oxygen species will interact with these gas molecules and release trapped electrons back to the conduction band. The performance index of a gas sensor, factors such as sensitivity, selectivity, thermal stability, and rate of response, are considerably influenced by shape, size, and surface morphology of the sensing material.

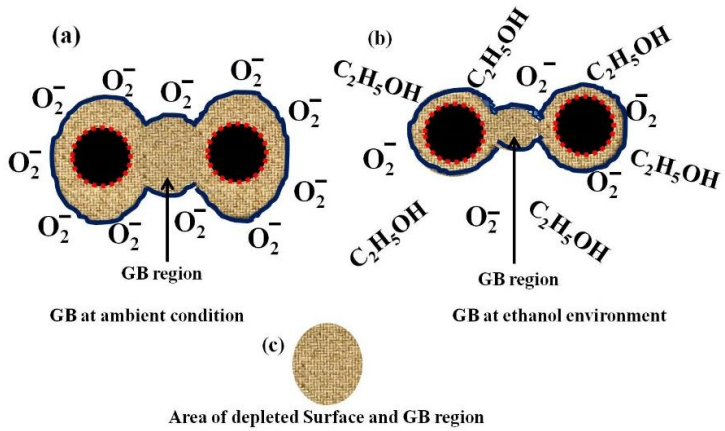

Fig. 8: (color online) Depleted region at GB (a) under ambient condition (b) under ethanol condition (c) surface and GB region around the grain.

In the sensor, ZnO depleted layers are formed in individual nanocrystallites as well as in grain boundary (GB) regions because the majority charge carriers are depleted due to the adsorption of oxygen molecules in ambient condition. Oxygen species from the atmosphere capture the free electrons at the surface of ZnO. Therefore, the negative charges of the film would be trapped at surface and grain boundary (GB) regions [Fig. 8(a)]. Trapping of negative charge causes the band bending upward. As a result, GB potential (φ_{GB}) and GB depletion width (ω)[Fig. 9(a)] are formed which control the carrier transport through the GB region. In the presence of deoxidizing gas like ethanol, electrons trapped by oxygen molecules are returned the ZnO film [Fig. 8(b)] and decreased the surface band bending [Fig. 9(b)] and increased the conductivity.

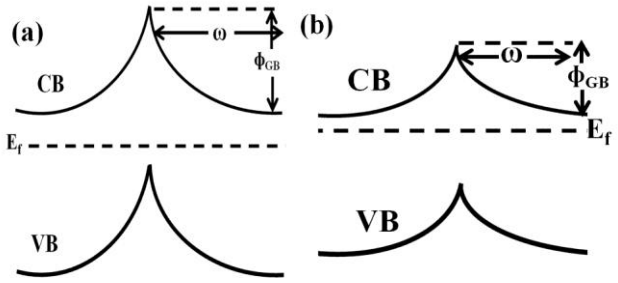

Fig. 9: GB potential ($\boldsymbol{\varphi_{GB}}$) and depletion width ($\boldsymbol{\omega}$) of ZnO under (a) ambient condition and (b) Ethanol environment.

CONCLUSION

The synthesis of spin coated ZnO and Mn doped ZnO thin films allowed us to develop a sensitive and robust gas sensor for ethanol detection. XRD results revealed ZnO films were polycrystalline with preferred orientation along (100), (002) and (101). SEM images illustrate grainy-like ZnO surfaces with the decrease in crystallite size for Mn doped ZnO films. EDX analysis revealed the presence of Zn, O, and Mn into the prepared films. The direct band gap energy was found to be decreased from 3.28 eV for undoped to 3.13 eV for 5% Mn doped ZnO. The sensitivity measurement with ethanol vapor showed the operating temperature of 160^{o}C for 3% Mn doped ZnO film. This temperature is found to be lower than reported value for similar systems.

ACKNOWLEDGEMENTS

We would like to thank the International Science Program (ISP), Uppsala University, Sweden for chemicals and equipment under the NEP 01 grant. The authors would like to acknowledge University Grants Commission for partial financial support in completing this work. S. Dhakal acknowledges the financial support from Virginia Commonwealth University (VCU Startup Grant).

REFERENCES

[1] Fu, L.; You, S.; Li, G.; Li, X. and Fan, Z. Application of semiconductor metal oxide in chemiresistive methane gas sensor: recent developments and future perspectives. *Molecules*, **28:** 6710-6735 (2023).

[2] Strle, D.; Stefane, B.; Trifkovic, M.; Miden, M.; Kvasic, I.; Zupanic, E. and Musevic, I. Chemical selectivity and sensitivity of a 16-channel electronic nose for trace vapour detection. *Sensors*, **17:** 2845-2869 (2017).

[3] Wang, J.; Yang, J.; Han, N.; Zhou, X.; Gong, S.; Yang, J.; Hu, P. and Chen, Y. Highly sensitive and selective ethanol and acetone gas sensors based on modified ZnO nanomaterials. *Materials and Design*, **121:** 69-76 (2017).

[4] Stehr, J. E.; Chen, S. L.; Filippov, S.; Devika, M.; Reddy, N.; Tu, C.; Chen, W. M. and Buyanova, I. A. Defect properties of ZnO nanowires revealed from an optically detected magnetic resonance study. *Nanotechnology*, **1583:** 272- 278 (2014).

[5] Asif, N.; Amir, M. and Fatma, T. Recent advances in the synthesis, characterization and biomedical applications of zinc oxide nanoparticles. *Bioprocess and Biosystems Engineering*, **46:** 1377-1398 (2023).

[6] Vyas, S. A short review on properties and applications of zinc oxide based thin films and devices. *Johnson Matthey Technology Review*, **64:** 202-218 (2020).

[7] Lian, Q.; Chen, M.; Mokhtar, M.; Wu, S.; Zhu, M.; Whittaker, E.; O'Brien, P. and Saunders, B. Surface structure, optoelectronic properties and charge transport in ZnO nanocrystal/MDMO-PPV multilayer films. *Physical Chemistry Chemical Physics*, **20:**12260-12271 (2018).

[8] Basyooni, M. A.; Shaban, M. and El Sayed, A. M. Enhanced gas sensing properties of spin-coated Na-doped ZnO nanostructured films. *Science Report*, **7:**41716-41728 (2017).

[9] Bhati, V.; Hojamberdiev, M. and Kumar, M. Enhanced sensing performance of ZnO nanostructures-based gas sensors: A review. *Energy Reports*, **6:**46-62 (2020).

[10] Reyes, A.; Rivera, M.; Chavez, H.; Martinez, H. and Medina, D. Recent advances in ZnO-based carbon monoxide sensors: role of doping. *Sensors*, **21:** 4425 (2021).

[11] Poloju, M.; Jayababu, N. and Reddy, M.V. Improved gas sensing performance of Al doped ZnO/CuO nanocomposite based ammonia gas sensor. *Materials Science and Engineering*, **227:** 61-67 (2018).

[12] Bisht, R. S.; Ghimire, R. R. and Raychaudhuri, A.K. Control of grain boundary depletion layer and capacitance in ZnO thin film by a gate with electric double layer dielectric. *The Journal of Physical Chemistry C*, **119**(49): 27813-27820 (2015).

[13] Sommer, N.; Hupkes, J. and Rau, U. Field emission at grain boundaries: modeling the conductivity in highly doped polycrystalline semiconductors. *Physical Review Applied*, **5:** 024009 (2016).

[14] Sugianto, S.; Nurilhilmah, N.; Darsono, T.; Sugiyanto, S.; Aryanto, D. and Isnaeni, I. Blue luminescence of indium-doped ZnO thin films prepared by DC magnetron sputtering. *Journal of Physics: Conference Series*, **1968:**012045 (2021).

[15] Hamelmann, F. U. Thin film zinc oxide deposited by CVD and PVD. *Journal of Physics: Conference Series*, **764:**012001-012009 (2016).

[16] Verardi, P.; Dinescu, M. and Andrei, A. Characterization of ZnO thin films deposited by laser ablation in reactive atmosphere. *Applied Surface Science*, **96:**827-830 (1996).

[17] Aryanto, D.; Jannah, W.N.; Masturi; Sudiro, T.; Wismogroho, A. S.; Sebayang, P.; Sugianto and Marwoto, P. Preparation and structural characterization of ZnO thin films by sol-gel method. *Journal of Physics: Conference Series*, **817:** 012025-012032 (2017).

[18] Khaleel, R.; Hashim, M. and Majeed, S. Synthesis of ZnO thin film by chemical spray pyrolysis using its nano powder. *Kuwait Journal of Science*, **49:**1–11 (2022).

[19] Sun, K.; Wei, W.; Ding, Y.; Jing, Y.; Wang, Z. L. and Wang, D. Crystalline ZnO thin film by hydrothermal growth. *Chemical Communication*, **47:**7776-7778 (2011).

[20] Mulmi, D. D.; Dhakal, A. and Shah, B. R. Effect of annealing on optical properties of zinc oxide thin films prepared by homemade spin coater. *Nepal Journal of Science and Technology*, **15:**111-116 (2014).

[21] Laurenti, M. and Cauda, V. Porous Zinc Oxide Thin Films: Synthesis Approaches and Applications. *Coatings*, **8**(2): 67-91 (2018).

[22] Narayanan, N. and Kannoth, D. Exploring p type conductivity in ZnO thin films by In-N cooping for homo-junction devices. Journal of Materials Science: *Materials in Electronics*, **28**: 5962-5970 (2017).

[23] Zhu, Z.; Kao, C. T. and Wu, R. J. A highly sensitive ethanol sensor based on $Ag@TiO_2$ nanoparticles at room temperature. *Applied Surface Science*, **320:** 348-386 (2014).

[24] Vladut, C.; Mihaiu, S.; Tenea, E.; Preda, S.; Moreno, J.; Anastasescu, M.; Stroescu, H.; Atkinson, I.; Gartner, M.; Moldovan, C. and Zaharescu, M. Optical and piezoelectric properties of Mn-doped ZnO films deposited by Sol-gel and hydrothermal methods. *Journal of Nanomaterials*, **2019:** 1-13 (2019).

[25] Ahmed, S. A. Structural, optical, and magnetic properties of Mn-doped ZnO samples. *Research in Physics*, **7:** 604-610 (2017).

[26] Shatnawi, M.; Alsmadi, A. M.; Bsoul, I.; Salameh, B.; Mathai, M.; Alnawashi, G.; Alzoubi, G. M.; Al-Dweri, F. and Bawaaneh, M.S. Influence of Mn doping on the magnetic and optical properties of ZnO nanocrystalline particles. *Research in Physics*, **6:** 1064-1071 (2016).

[27] Bak, S.; Lee, J.; Kim, Y. and Lee, S. Sensitivity improvement of Urchin-like ZnO nanostructures using two-dimensional electron gas in MgZnO/ZnO. *Sensors*, **19:** 5195 (2019).

[28] Chaudhary, D. K.; Maharjan, Y. S.; Shrestha, S.; Maharjan, S.; Shrestha, S. P. and Joshi, L. P. Sensing performance of a ZnO-based Ammonia Sensor. *Journal of Physical Science*, **33**(1): 97-108 (2022).